BILINGUAL PUBLISHING GROUP

Journal of Atmospheric Science Research

https://journals.bilpubgroup.com/index.php/jasr/index

ARTICLE

Control of the Dust Vertical Distribution over Western Africa by Convection and Scavenging

H. Senghor[1*], R. Pilon[3], B. Diallo[3], J. Escribano[4], F. Hourdin[3], J. Y. Grandpeix[3], O. Boucher[3], M. Gueye[6], A. T. Gaye[2], E. Machu[5]

[1] *National Agency of Civil Aviation and Meteorology, PO BOX 8184, Senegal*
[2] *Laboratory for Atmospheric-Oceanic Physics-Simeon Fongang, Cheikh Anta Diop University, Dakar, 10700, Senegal*
[3] *Laboratory of Dynamic Meteorology (LMD), CNRS/IPSL/UMPC, Paris, 75231, France*
[4] *Atmospheric Composition Group, Barcelona Supercomputing Center (BSC), Barcelona, 08034, Spain*
[5] *Spatial and Physical Oceanography Laboratory (LOPS), Brest University, CNRS, IRD, Plouzane, 29280, France*
[6] *Department of Mathematics and Computer Science, University of Sine Saloum El Hadj Ibrahima Niasse, PO BOX 55, Kaolack, Senegal*

ABSTRACT

Saharan dust represents more than 50% of the total desert dust emitted around the globe and its radiative effect significantly affects the atmospheric circulation at a continental scale. Previous studies on dust vertical distribution and the Saharan Air Layer (SAL) showed some shortcomings that could be attributed to imperfect representation of the effects of deep convection and scavenging. The authors investigate here the role of deep convective transport and scavenging on the vertical distribution of mineral dust over Western Africa. Using multi-year (2006–2010) simulations performed with the variable-resolution (zoomed) version of the LMDZ climate model. Simulations are compared with aerosol amounts recorded by the Aerosol Robotic Network (AERONET) and with vertical profiles of the Cloud-Aerosol Lidar with Orthogonal Polarization (CALIOP) measurements. LMDZ allows a thorough examination of the respective roles of deep convective transport, convective and stratiform scavenging, boundary layer transport, and advection processes on the vertical mineral dust distribution over Western Africa. The comparison of simulated dust Aerosol Optical Depth (AOD) and distribution with measurements suggest that scavenging in deep convection and subsequent re-evaporation of dusty rainfall in the lower troposphere are critical processes for explaining the vertical distribution of desert dust. These processes play a key role in maintaining a well-defined dust layer with a sharp transition at the top of the SAL and in establishing the seasonal cycle of dust distribution. This vertical distribution is further reshaped offshore in the Inter-Tropical Convergence Zone (ITCZ) over the Atlantic Ocean by marine boundary layer turbulent and convective transport and wet deposition at the surface.

Keywords: Dust; Vertical distribution; Sahara; Sahel; West Africa; Climate model; Convection; Scavenging; ITCZ

*CORRESPONDING AUTHOR:
Habib Senghor, National Agency of Civil Aviation and Meteorology, PO BOX 8184, Senegal; Email: habib.senghor@ucad.edu.sn

ARTICLE INFO
Received: 10 October 2023 | Revised: 21 December 2023 | Accepted: 26 December 2023 | Published Online: 8 January 2024
DOI: https://doi.org/10.30564/jasr.v7i1.6009

CITATION
Senghor, H., Pilon, R., Diallo, B., et al., 2024. Control of the Dust Vertical Distribution over Western Africa by Convection and Scavenging. Journal of Atmospheric Science Research. 7(1): 19–39. DOI: https://doi.org/10.30564/jasr.v7i1.6009

1. Introduction

North Africa is the world's largest source of dust with more than 55% of global dust emissions [1] and approximately 60% of this dust is transported from these arid and semi-arid emission areas across the Atlantic Ocean [2,3]. Mineral dust is known to negatively impact the West African economy [4] and human health in the Sahelian region [5]. It has been associated with mortality during warmer months in Mediterranean cities [6]. Long-range transport of Saharan dust is widely known as reported by Zanobetti and Schwartz (2009) for the United States: Saharan dust can intrude into the Caribbean Basin and the northern American continent after being lifted into the atmosphere by winds over West Africa and then transported across the Atlantic Ocean within the Saharan Air Layer [7]. Dust affects the local energy balance and modifies the hydrological cycle [8] through aerosol-radiation and aerosol-clouds interactions [3,9], but also through changes in atmospheric stability by absorption of solar radiation and surface thermal radiation [10]. Seasonal dust emission variability is highly driven by the variability of surface winds and in particular by variations in the low-level jet responsible for the maximum surface wind that occurs when momentum is transported downward to the surface by boundary layer convection [11,12]. In early summer, turbulence and high winds surface can raise heavy dust loading especially at the leading edge of the cold pool outflows from downdrafts of moist convection when the evaporating rainfall cools the air in the subcloud layer [13]. Dust storms induced by cold pool outflows are called "haboob" (a violent dust storm or sandstorm). This mechanism allows air mass to sink to the surface, particularly if the environment is dry adiabatic [14]. Furthermore, deep convection impacts the aerosol vertical distribution, which is also controlled by atmospheric transport and scavenging [15–17]. Considerable efforts have been made to study the role of aerosols in the Earth system [18] and more specifically over West Africa [19–21].

Recent modeling studies have shown that the dust cycle (defined as the emission, transport, and deposition of dust) depends on weather conditions and is highly sensitive to the removal by atmospheric hydrometeors [22]. Modeling has helped to narrow uncertainties in the spatial distribution of aerosols at the global scale [12,23–25]. Given the size of the domain involved in dust propagation, General Circulation Models (GCMs) are often used to tackle the dust problem and are used for a full description of all stages of its atmospheric lifecycle [26].

Nonetheless, models need to be improved to represent the vertical transport of dust to better explain the mechanisms controlling the aerosol vertical redistribution of dust over the Sahelo-Saharan region. For dry deposition, it is a common practice to choose a constant deposition velocity of aerosol in the first layers of the model for fine particles. The sedimentation or gravitational settling is usually estimated from simple parameterizations that can lead to the large spread in aerosol residence time shown in model intercomparison studies [27]. The sensitivity of the representation of aerosol vertical profiles and their physical processes is, to our knowledge, poorly studied in the literature. Additionally, particle size distribution, optical properties, and dust shape and composition are still poorly represented in models [28,29].

Representing the effects of transport and clouds is even more challenging. To address this problem, some authors have used terragenic (^{210}Pb) and cosmogenic (^{7}Be) aerosol tracers to estimate the impact of the removal of aerosol in the atmosphere by the convective and stratiform precipitations in GCMs [17,30–32].

We build on the inspiring effort by Pilon et al. (2015) to better represent the transport of dust and scavenging in the deep convective scheme in the LMDZ model in order to show the vertical structure of dust distribution in the SAL, over the Western Africa region, and its control by convective transport and scavenging.

This study provides additional insights into the convective transport and scavenging of Saharan dust through quantitative diagnostics of dust distribution and through the assessment of the contribution of

each physical process involved in this distribution. For this purpose, we use the new configuration of the LMDZ model coupled online with the Simplified Aerosol Model [12,24].

Section 2 introduces the model and describes the contribution of physical processes of dust transport in the LMDZ model. The methodology and the validation dataset are presented also in this section. Section 3 is devoted to the analysis of the results and the effects of the transport and scavenging of dust by convective processes. Finally, we discuss results in Section 4 and draw general conclusions in Section 5.

2. Experimental design

2.1 Climate modeling

The work presented here relies on the Laboratoire de Météorologie Dynamique GCM LMDZ version 6A [33], and more specifically the version used for the sixth Coupled Model Intercomparison Project (CMIP6) simulations. This model version includes a new set of physical parameterizations called "New Physics" addressing particular convective clouds. The parameterization of deep convection uses a modified version [34] of Emanuel's mass-flux scheme [35] coupled to a specific parameterization of cold pools [36,37] and to a stochastic triggering designed to make the frequency of occurrence of new convective systems within a mesh aware of the grid cell size [38]. The boundary layer convection is represented by the thermal plume model. It is described in Hourdin et al. (2019) [39] and now accounts for stratocumulus clouds. Large-scale condensation processes follow the work of Le Treut and Li (1991) [40]. This model version also includes the introduction of the latent heat release associated with water freezing and a new parameterization of non-orographic gravity waves targeting the representation of the Quasi-Biennial Oscillation (QBO). LMDZ has the particular ability to allow the deformation of its horizontal grid to focus on a region of interest [41,42].

LMDZ also allows the transport of an arbitrary number of tracers such as dust here. In this work, dust is considered as a tracer and is dealt with as any other tracer. An overview of tracer transport in the LMDZ climate model is provided by Heinrich and Jamelot (2011). A more detailed description is given in Section 2.3. Specific work was dedicated to the introduction of convective transport and scavenging in the Emanuel convective scheme and the modification of the large-scale condensation scavenging [17].

The LMDZ model is run here at a resolution of 1° × 1° over the domain 70°W–70°E; 0°N–40°N (the zoom is centered at 5°W, 19°N), with 39 hybrid sigma coordinate levels. The Simplified Aerosol Model (detailed in the next subsection) is embedded in LMDZ and provides the capability to represent different dust bins, their emission, lifting, and deposition.

Two five-year simulations have been performed after 10 years of spin-up as in Wang et al. (2018) [43] to reach groundwater table stability in the Organising Carbon and Hydrology in Dynamic Ecosystems (ORCHIDEE) land surface model coupled to LMDZ6A [44,45]. Both simulations only differ by the activation of large-scale and convective scavenging. These simulations are here in after referred to as NOSCAV and SCAV, respectively (**Table 1**). The Simulation with Scavenging (SCAV) serves as a control case. The time step for the computation of physic parameterization is 15 minutes in both simulations.

Owing to the constraints of computer time and the project timeline, only one LMDZ simulation has been performed for each configuration. The two simulations cover the period 2006–2010 when the observational measurements from African Monsoon Multidisciplinary Analysis (AMMA) were fully operational [46]. Horizontal winds were relaxed towards the European Centre for Medium-Range Weather Forecasts (ECMWF) ERA-Interim reanalysis [47], with a 48 h time relaxation in the zoom area and 3 h outside the grid-box as in Hourdin et al. (2015) [12]. Although ERA-Interim has been discontinued and replaced by ERA-5 reanalysis [48], the latter was not

available at the time the simulation was made. Test runs were performed using ERA-5 reanalysis wind but no significant difference was seen.

Table 1. LMDZ model with simulations period and NP package with and without scavenging, respectively.

Simulations	Configurations	Period (years)
SCAV	NP + Scavenging	2006–2010
NOSCAV	NP + No scavenging	

2.2 Aerosol model

We use the Simplified Aerosol Model (SPLA), originally developed by Huneeus et al. (2009) SPLA is an aerosol model of intermediate complexity that is fully embedded in the LMDZ model and has been used to estimate global aerosol emissions [49].

Escribano et al. (2016) have made the original version of SPLA compatible with LMDZ6A used in this research work. Thus, the aerosol model includes surface emissions and dust particles released by the evaporation cloud process, dry deposition, scavenging, convective transport, boundary layer mixing, transport from subgrid-scale thermals [12], and sedimentation for coarse mode aerosols [24].

The configuration of SPLA used here represents aerosols with five tracers: aerosol precursors (lumped together as a single species), fine aerosols, coarse sea salt aerosols with diameters ranging from 1–40 μm, and two coarse modes of desert dust. Dust thus contributes to three different bins: The Super Coarse Dust (SCDU) corresponds to diameters ranging from 6–30 μm, the Coarse or Intermediate Dust (CODU) to diameters ranging between 1 and 6 μm, and the Fine Particles (FINE) include to dust particles with diameters smaller than 1 μm [24]. They are listed in **Table 2**. In this study, emissions of aerosols other than dust are set to null. Fine aerosol thus consists only of dust fine mode. The emission scheme is adapted from the CHIMERE-Dust air quality model [50]. The dust production model is composed essentially of a saltation flux scheme from Marticorena and Bergametti 1995 [51] and a sandblasting model from Alfaro and Gomes (2001) [52]. Threshold friction velocities are estimated following Shao and Lu (2000) [53] and corrected by a drag efficiency coefficient [54]. SPLA contains the different coefficients for aerosol types.

The SPLA model relies on the land surface model to compute the stocks of water and carbon in the different soil and plant reservoirs, which the emission scheme depends upon.

Large-scale scavenging is composed of in-cloud (nucleation), below-cloud (impaction), and evaporation. The efficiency of in-cloud scavenging for dust aerosols is set to a value of 0.7 as in LMDZ, meaning that 30% of the dust aerosols are assumed to remain interstitial in the cloud. No distinction is made between hydrophilic and hydrophobic aerosols [55]. Below-cloud impaction efficiency is set to 0.5 [17,56].

Table 2. Dust size bins in the SPLA model.

Mineral dust	FINE	CODU	SCDU
Size (μm)	< 1	1–6	6–30

2.3 Representation of atmospheric transport

We recap here the treatment of LMDZ (and also the SPLA model) with dust transport, scavenging and the decomposition of tracer transport in its various contributions.

At each model time step, the tracer concentration in one grid cell is affected by the effects of the large-scale advection (computed with a second-order finite-volume; see Hourdin and Armengaud, 1999 [57] and of the various physical parameterizations that can affect tracers. The total tracer q tendency reads,

$$(\partial_t q)_{total} = (\partial_t q)_{adv} + (\partial_t q)_{phy} \quad (1)$$

where $(\partial_t q)_{adv}$ is the effect of large-scale advection and $(\partial_t q)_{phy}$ is the total effect of the physical parameterization. This physical tendency can be further decomposed as:

$$(\partial_t q)_{phy} = (\partial_t q)_{turbl} + (\partial_t q)_{therm} + (\partial_t q)_{cv} + (\partial_t q)_{lsscav} + (\partial_t q)_{sed} \quad (2)$$

where $(\partial_t q)_{turbl}$ denotes the transport induced by the turbulent diffusion in the atmospheric boundary layer, $(\partial_t q)_{therm}$ is the tendency induced by the ther-

mal plume model, $(\partial_t q)_{cv}$ denotes the transport and the scavenging by the Emanuel convection scheme, $(\partial_t q)_{lsscav}$ is the tendency induced by the large-scale scavenging, and finally, $(\partial_t q)_{sed}$ denotes the effect of tracer sedimentation. Each temporal variation of tracer concentration in the model physics is detailed below.

The turbulent transport in the planetary boundary layer is treated as a vertical diffusion with an eddy diffusivity *Kz* computed from the turbulent kinetic energy prognostic equation that follows Yamada (1983) [58].

The effect of large-scale scavenging is as follows:

$$(\partial_t q)_{lsscav} = (\partial_t q)_{ls,nucleation} + (\partial_t q)_{ls,impaction} + (\partial_t q)_{ls,evap} \quad (3)$$

where $(\partial_t q)_{ls,nucleation}$ is proportional to the conversion rate of cloud water into precipitation and the cloud fraction. The nucleation model is a modification from Reddy and Boucher (2004) [56] and aims to follow closely the large-scale condensation parameterization; $(\partial_t q)_{ls,impaction}$ is proportional to the precipitation flux and takes into account the impaction efficiency of raindrops and snowflakes;0 $(\partial_t q)_{ls,evap}$ depends on the precipitation flux. Each of these three tendencies is detailed in the appendix of Pilon et al. (2015) [17].

Dry deposition flux to the ground is assumed to be proportional to the aerosol concentration in the lowest model layer and to a prescribed velocity respectively of 0.1 cm. s^{-1} for FINE dust mode and 1.2 cm.s^{-1} for coarse dust [55].

Finally, deep convection affects the tracer distribution through both transport and scavenging in both the saturated and unsaturated drafts (which are separated by (1) precipitating water and (2) the air flowing down in the draft) constituting the mass fluxes of Emanuel's scheme. For analysis and in contrast to the study of Pilon et al. (2015) [17], we split the effect of deep convection on the tracer distribution into three tendencies reflecting the scavenging in saturated drafts $(\partial_t q)_{cvsscav}$, the scavenging in unsaturated drafts $(\partial_t q)_{cvunscav}$, and the deep convective transport by both drafts $(\partial_t q)_{cvtrsp}$.

$$(\partial_t q)_{cv} = (\partial_t q)_{cvtrsp} + (\partial_t q)_{cvsscav} + (\partial_t q)_{cvunscav} \quad (4)$$

2.4 Validation data

We compare simulated monthly mean AOD computed from the daytime averaged AOD between 2006 and 2010 to the observed AOD from AERONET sun photometers [59,60] (**Figure 1**). We also use the Level 2 product of Cloud-Aerosol Lidar and Infrared Pathfinder Satellite Observations (CALIPSO) launched on 28 April 2006 [61,62]. CALIPSO flies as part of the International Afternoon Constellation (A-Train) and provides global coverage of clouds and aerosol properties [63]. The latter are optical and physical properties obtained from the CALIOP onboard CALIPSO. The Vertical Feature Mask (VFM) algorithm is used to discriminate clouds and aerosol types [64,65]. We use CALIOP data from June 2006 to December 2010. We then compute the Dust Occurrence Frequency (DOF) using the same method found as in Adams et al. (2012) and Senghor et al. (2017) [65,66]:

$$DOF(x,y,z) = \frac{\sum_{n=0}^{N} p_n(x,y,z)}{\sum_{n=0}^{N} s_n(x,y,z)} \forall x,y,z \quad (5)$$

where p is the occurrence probability of dust at a grid point of longitude x, latitude y, and altitude z. s is the total number of valid satellite tracks in the grid-box, and N is the total number of grid points. The occurrences in the longitude (x) are summed and normalized by the total valid satellite tracks in the range 35°W–10°E using Equation (5). A horizontal grid spacing of 0.5° × 0.5° is used for grid data. The vertical resolution is 30 m for 290 vertical levels between –0.5 and 8 km above sea level. For the retrieval of the extinction coefficient from CALIOP, a Lidar ratio is required to be used for the aerosol type. Schuster et al. (2012) emphasized that the Lidar ratio shows a significant variability within the Sahara region [67]. Gasteiger et al. (2011) have shown that the Lidar ratio may also strongly depend on the shape and size of particles [28]. To avoid this dependency, we use qualitative information with the VFM for the estimation of the DOF as in Tsamalis et al. (2013) [68]. We are using the dust mass concentrations for the size bins with diameters ranging from 0.01–30 μm [24] to calculate the mineral dust occurrence for latitudinal cross-sections 12°–21°N in the model. We

use mass concentrations from the model outputs to compute the probability of DOF in the LMDZ model at each grid point when CALIPSO overpasses our domain between 10:00 and 15:00 UTC like all satellites in the Afternoon constellation (A-Train). For each valid satellite track, the dust occurrence is defined by the number concentration at each grid point if the mass concentration is larger than the threshold of 2.65 $g.cm^{-3}$ and 0 otherwise [69]. The probability is obtained when this number is divided by the sum of the number concentration in the grid box [65,67,68]. We have calculated the vertical coordinate of the model in km as in Wallace and Hobbs (2006) [70].

3. Results

We present here the assessment of the LMDZ/SPLA model in terms of AOD and vertical distribution of dust. We show the effect of the activation of scavenging by comparing two simulations: A control simulation where the scavenging is activated, and another one without activation of the scavenging (see **Table 1**). We also discuss the importance of the various components of the large-scale and parameterized vertical transport by decomposing this transport according to Equation (4).

3.1 Comparison of simulated and observed AOD

To assess the column-integrated aerosol amount simulated by the model, we made a comparison of the AOD at 550 nm between SCAV/NOSCAV simulations, and AERONET measurements [59]. As discriminated in Senghor et al. 2017 observed that AOD for dust is defined by using the Angstrom Exponent (AE) [65]. Only mineral dust is considered in the calculation of AOD from the SCAV and NOSCAV simulations. The comparison is made at different stations of the AERONET network in the Sahel region: Banizoumbou [13.54°N, 2.66°E] (**Figure 1b**), Agoufou [15.34°N, 1.47°W] (**Figure 1a**), Cinzana [13.27°N, 5.93°W] (**Figure 1c**) and Dakar [14.39°N, 16.95°W] (**Figure 1d**). The AERONET data show a clear annual cycle over the Sahel with a bimodal structure. The highest values of AOD are 0.6 and 0.7 for March and June in Dakar and Cinzana, respectively. Over Agoufou and Banizoumbou, the maximum is obtained respectively in June and April with a slightly higher value of AOD (0.8). The SCAV simulation reproduces a seasonal cycle of AOD in agreement with observations in West Africa with a maximum atmospheric aerosol loading in the dry season and a minimum AOD in the rainy season. The model underestimates slightly the AOD over Banizoumbou, Cinzana, and Agoufou in the dry season when the contribution of the biomass burning is maximum over Guinea Golf countries [71] and overestimates AOD over Dakar all along the year. The AOD from the SCAV simulation is similar to the observation during the summer and autumn seasons. By comparison, the NOSCAV strongly overestimates the atmospheric dust loading (AOD of 2 to 2.5) and shows a maximum in July–August. In July, the largest values of observed AOD (**Figure 1**) are also simulated in the model as well as the intensification of the westward dust transport in the SAL. Overall, **Figure 1** shows that the model is able to detect and reproduce the most active dust sources established from field campaigns over West Africa [71].

To further assess the spatial distribution of modeled dust aerosols (**Figures 2a, 2b, 2e and 2f**), Deep Blue AOD at 550 nm from Modis/Terra product (**Figures 2c and 2d**) is used for quantitative validation. In January, the transport of dust plume observed by the satellite between 0° and 20°N is well reproduced by the model as well as the active source located southwest of Mauritania close to the border with Senegal (**Figures 2a, 2c, and 2e**). The detection of these sources is missed by the satellite, but field campaigns, such as the Saharan Aerosol Long-Range Transport and Aerosol-Cloud-Interaction Experiment [71]; **Figure 5** shows that this location contains one of the most active dust sources in Western Africa. The model is in reasonable agreement with CALIPSO observation which shows a reinforcement of the dust layer on both sides, i.e. land and ocean (**Figure 3a**). In July, heavy atmospheric dust loading is observed by Modis (**Figure 2d**) between 10° and 25°N. **Figures 2b and 2f** show that, both models reproduce the strong seasonal change in the airborne

dust over Sahel as observed by satellites.

3.2 Vertical structure of the Saharan air layer

The vertical distribution of observed and simulated mineral dust in West Africa (band of latitude 12°–21°N) is marked by a strong seasonal variability (**Figure 3**). More dust is suspended in the atmosphere during boreal summer than during winter over the whole LMDZ domain. This seasonal cycle is shown by observations (**Figures 3a and 3c**) and is well captured by the model (**Figures 3b and 3d**). The larger dust occurrence obtained in summer is due to the stronger activity of the North African dust sources as shown by satellite observations and different field campaigns [71–73]. In winter, the vertical distribution of dust in the longitude band 12°–17°W is limited between the surface and 3 km and shows a maximum of dust occurrence between the surface and 2 km (**Figure 3a**). The experiment SCAV exhibits a maximum occurrence of dust in the same longitudinal cross-sections, but at a lower altitude and over a thinner atmospheric boundary layer less than the observations (**Figure 3b**). At the transition zone between the continent and the Atlantic Ocean (17°W; black dashed line in **Figure 3**), the dust layer is in contact with the ocean surface and the model can reproduce this structure of the dust layer. In summer, observations show that mineral dust is vertically distributed between the surface and 6 km, with a significant dust occurrence between 2 and 5 km (**Figure 3c**) within the SAL [65,68,74]. For both seasons, the NOSCAV simulation shows heavier atmospheric dust loading than model SCAV and observations (**Figures 3f and 3e**). At the transition zone (17°W), the Lidar measurements show a vertical discontinuity of dust layers between land and ocean surfaces. The dust in the model extends less in altitude and the occurrences are slightly higher but the vertical structure is well preserved. The model is also capable of reproducing the structure of the dust layer at the transition zone between land and ocean. In the following section, we will explain the mechanisms that control the elevation of dust layers over the ocean [65,66,68] and the westward dust transport away from the main dust sources and at the transition zone.

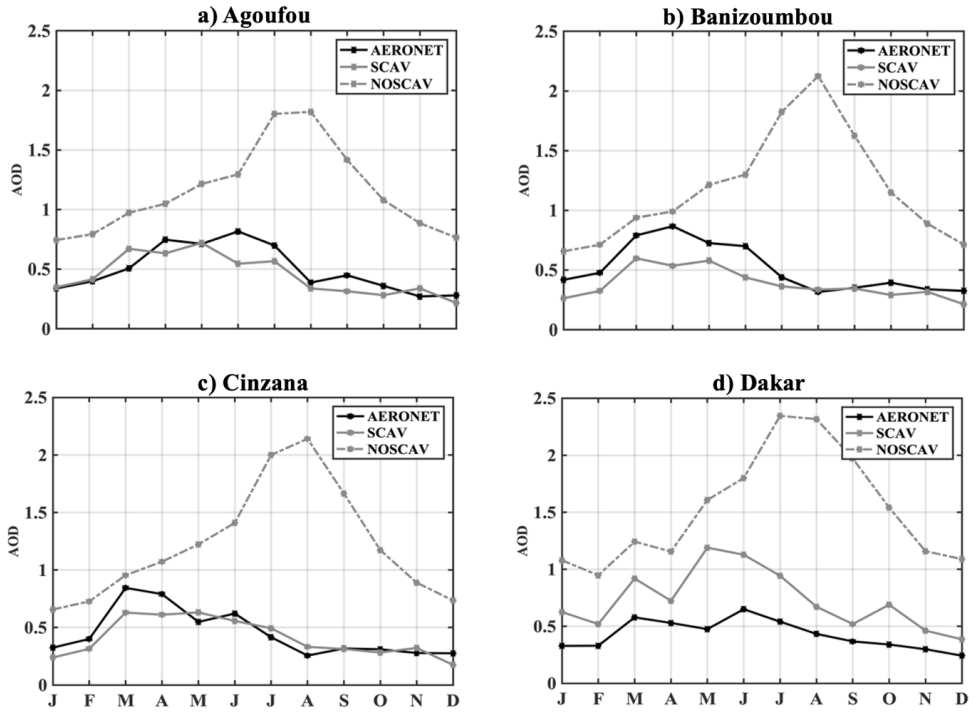

Figure 1. Modeled and observed monthly averaged AOD at 550 nm at four AERONET stations in the Sahel region (Agoufou (a), Banizoumbou (b), Cinzana (c) and Dakar (d)) during the period 2006–2010. The dashed gray line represents the AOD from the NOSCAV simulation, the solid gray line represents the SCAV simulation, and the black line is for AERONET data.

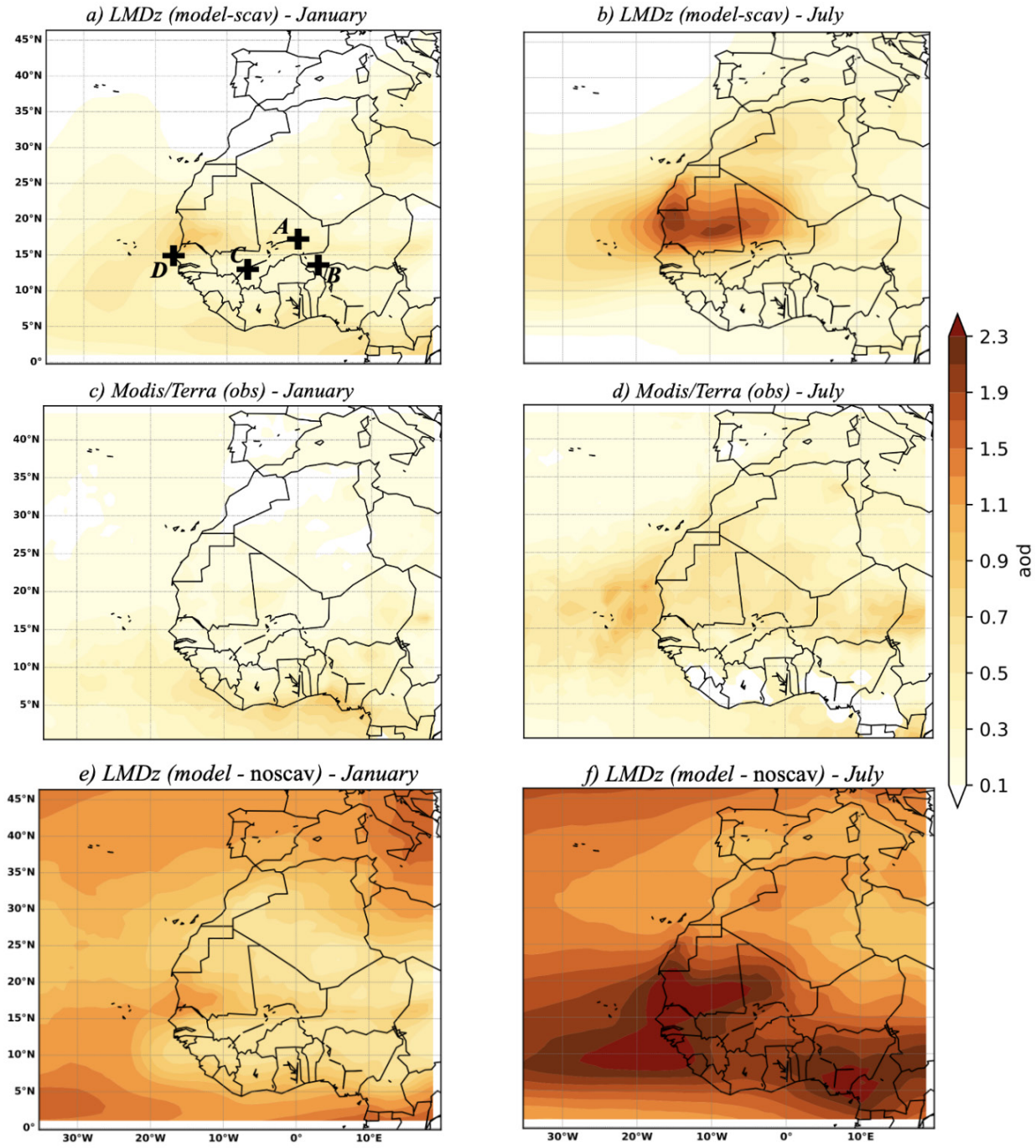

Figure 2. Monthly averaged spatial distributions of AOD at 550 nm, from 2006 to 2010 for January (left panels) and for July (right panels), in LMDZ simulations (a and b for SCAV; e and f for NOSCAV). c) and d) AOD retrievals from MODIS/Terra product and mapped onto the model grid. The A, B, C and D labels correspond to the AERONET stations in Agoufou, Banizoumbou, Cinzana and Dakar, respectively, all located in the Sahel region.

3.3 Control by the large-scale circulation

Figure 4 illustrates the seasonal variation of the vertical distribution of dust concentration over Western Africa. We averaged the two dust bins SCDU and FINE in the latitude range 16°W–10°E where the dust emission and transport occur in summer [46,71]. In January and over continents (**Figure 4**), the simulated wind field shows the Harmattan flux near the surface and a strong mass flux subsidence around 20°N, which blocks the vertical uplift of dust at 850 hPa. All sizes of dust are lifted over the Intertropical discontinuity by dry convection, but only the FINE mode is elevated in higher layers, up to 600 hPa at 0°N. The large-scale circulation is responsible for dust vertical transport over the continent in winter when the convergence of air masses from the Harmattan and the monsoon flux occurs, as described by Hamilton et al. (1945) and Stuut et al. (2005) [75,76]. South of 10°N, the vertical distribution of dust over West Africa is dominated by the convective updrafts in the ITCZ (**Figure 4a**). This strong vertical transport brings aerosols up to 600 hPa at the Equator. The Hadley cell plays an important role in controlling the dust vertical distribution by stopping the dust elevation at 850 hPa in the latitudinal range 20°–30°N. The westward transport of dust over the Atlantic Ocean induces an important dry deposition along the way with 90% of SCDU removed between land and Ocean (**Figures 4c and 3c**). The FINE concentration decreased by about 50% during their westward transport between 10°E and 35°W. The air subsidence associated with the Azores anticyclone blocks the elevation of the aerosol layers between 10° and 20°N but there is an important vertical transport of FINE between 0° and 10°S and 18°–35°W (**Figure 4c**) in agreement with observations [65,77,78]. As shown in **Figures 3a, 3b, and 3f**, a clear homogeneous transition of the vertical distribution of aerosols is seen between land and ocean with a dust layer in contact with the ocean surface (**Figure 4c**). In July, overland (**Figure 4b**), the maximum dust concentrations reach about 105 $\mu g.m^{-3}$ for the SCDU, 56 $\mu g.m^{-3}$ for CODU, and 5 $\mu g.m^{-3}$ for FINE. During summer, the effect of the Hadley cell on the dust vertical distribution is not as strong as in winter. The ITCZ signal is clear and intense in summer as shown by the strong wind of 0°–20°N (**Figure 4b**). The divergence of the air masses is located at 100 hPa in summer, whereas it occurs at 500 hPa in winter (**Figures 4b and 4a**). Above the dry convection in North Africa, the descending branch of the Hadley cell limits the vertical transport of desert dust at 500 hPa between 10° and 20°N in the model (**Figure 4b**). This is in agreement with previous studies based on observations [79–82]. The CODU and FINE concentrations decrease during their westward transport but less than for the SCDU particles (see Sections 3.4 and 3.5). The elevation of the dust layer located in the latitudinal cross-section 12°–20°N is similar to CALIOP observations (**Figures 3c–3d**). In the tropical eastern Atlantic basin (35°W–18°W), the maximum dust concentrations in the layer 2–5 km induce a weak dry deposition over the Ocean in both models as already underlined in Chiapello et al. (1995); Liu et al. (2012); Tsamalis et al. (2013) or Senghor et al. (2017) [65,68,83,84].

To further assess the vertical distribution of dust, vertical profiles of the simulated DOF are compared with observations in **Figure 5**. Both simulations can reproduce the altitude of the maximum DOF located around 3.5 km, but underestimate the redistribution of dust in the troposphere (from the surface to 3 km) overland, particularly in the SCAV simulation (**Figure 5a**). The NOSCAV simulation catches a maximum value similar to the observation of around 3.5 km. Both simulations are able to capture the inversion of DOF below 1 km and above 5 km overland (**Figure 5a**) as well as over the ocean (**Figure 5b**). Over the ocean, the two simulated DOF profiles show a distinct behavior compared to observations. The SCAV simulation appears to better simulate the DOF profile between 1.5 and 3.5 km where the maximum dust is observed (**Figure 5b**). However, both simulations underestimate the dust distribution above 4.5 km and from the surface to around 1 km.

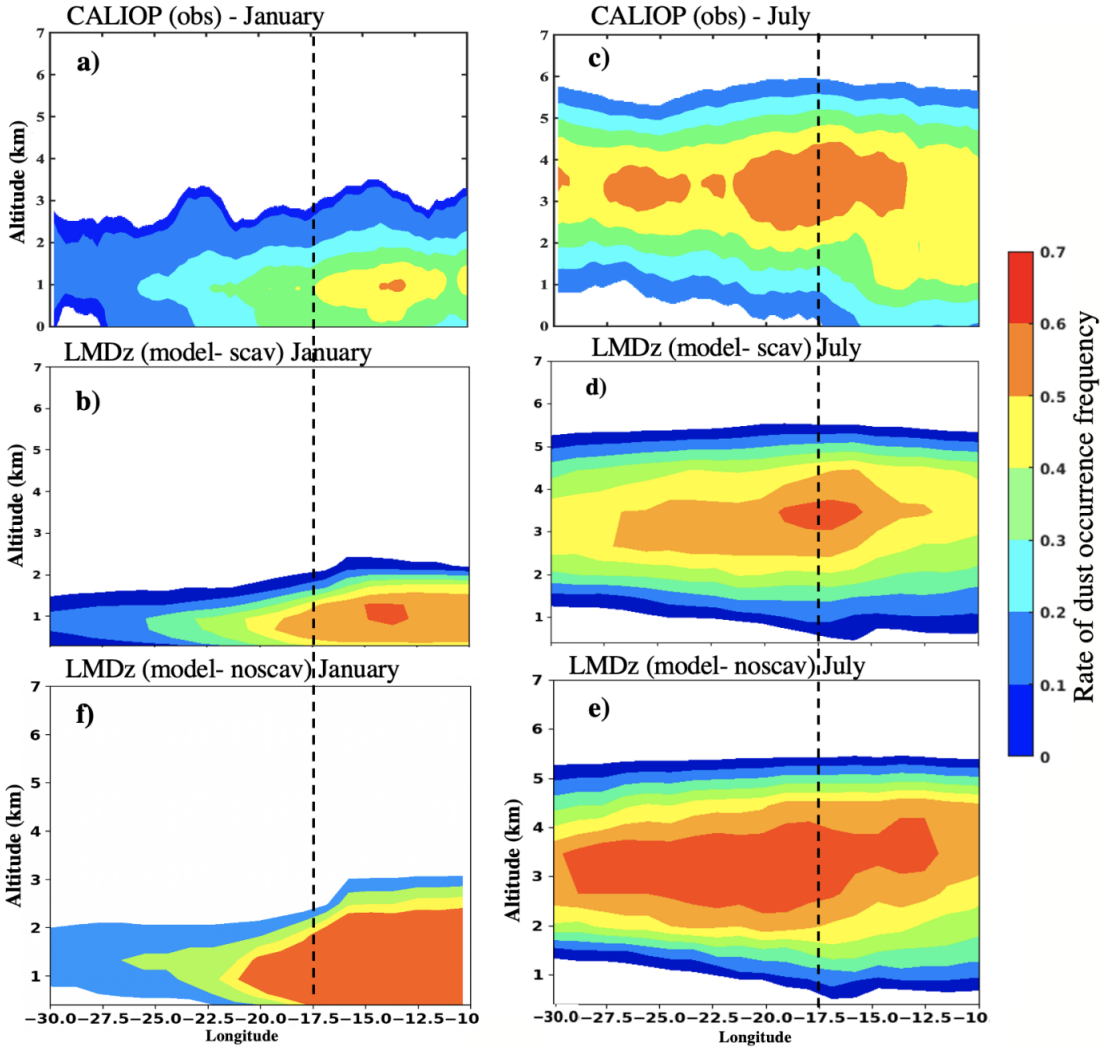

Figure 3. Vertical distribution of the dust aerosol occurrence frequency averaged over West Africa between latitudes 12°–21°N during January ((a) observations, (b) model (SCAV), and (f) model (NOSCAV)) and July ((c) observations, (d) model (SCAV), and (e) model (NOSCAV)). e) represents the vertical distribution of the dust occurrence with the NOSCAV simulation in July during the rainy season. The dust aerosol occurrence is averaged respectively for 5 years CALIPSO observations (2006–2010) and 5 years LMDZ model (2006–2010). The black dashed line represents the transitional zone between land and ocean.

3.4 Control of the vertical structure by physical processes

In this section, we focus our analysis on the processes impacting the dust vertical distribution in the troposphere. **Figure 6** shows the vertical profiles of the tendency of each model process (Equations (2), (3), and (4)) involved in the evolution of dust concentrations. In January, the boundary layer turbulence diffusion and thermal plume transport are the main processes enriching the lower atmosphere over the continent from 850 hPa to the surface (below 2 km). SCDU dust particles are removed by sedimentation which dominates the dry deposition below 850 hPa (**Figure 6a**). Dust is then transported westward over the ocean by advection (**Figure 6c**) between the surface level and 900 hPa (below 1 km). Note that the advection flux has a magnitude reaching approximatively 0.1 $g.kg^{-1}.day^{-1}$. Above the ocean, the large-scale scavenging redistributes the dust from 850 hPa (1.5 km) to the lower layers between 900 hPa and the surface (below 1km), and the thermal plume redistributes dust between 800 and 900 hPa (**Figure 6c**). Sedimentation and turbulence seem to withdraw dust from the lower atmosphere together with thermal plumes that slightly

enrich the surface layer (**Figure 6c**) in agreement with Friese et al., 2016 [85]. In January and above the coast (**Figure 6e**), the processes affect the dust distribution in a similar manner as over the ocean except for the thermal plumes above 500 m. Another subtle difference with the oceanic region is that the tendencies from advection, sedimentation, and thermals peak slightly lower.

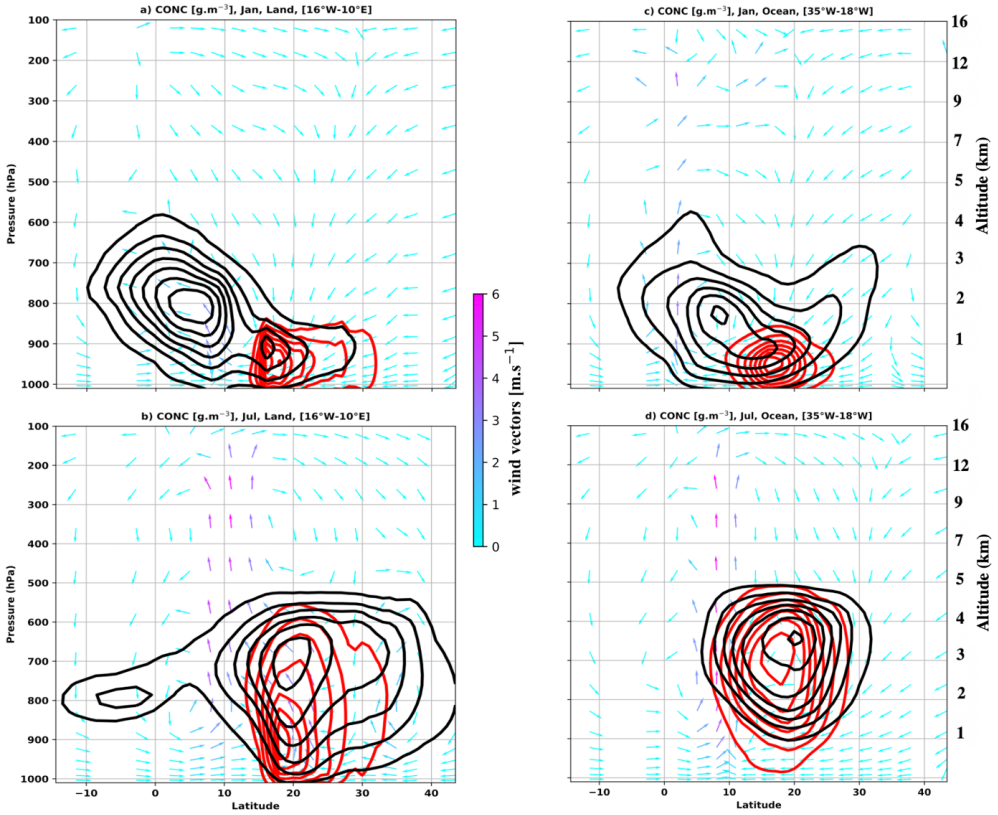

Figure 4. Vertical cross-sections (16°W–10°E) of aerosol concentration from SCAV, for the SCDU (red lines) and FINE (black lines) dust modes over West Africa and meridional wind (arrows; m/s) averaged over [16°W–10°E] for January (a, c) and July (b, d) between 2006 and 2010; Land (left; a, b) and Ocean (right; c, d). Dust concentrations (contours) are expressed in µg.m^{-3}. For the FINE mode, the black contour lines go from 0.5 to 5 µg.m^{-3} with a 0.5 µg.m^{-3} interval. For the SCDU mode red solid contour lines show values ranging from 15 to 105 µg.m^{-3} with a 25 µg.m^{-3} inter

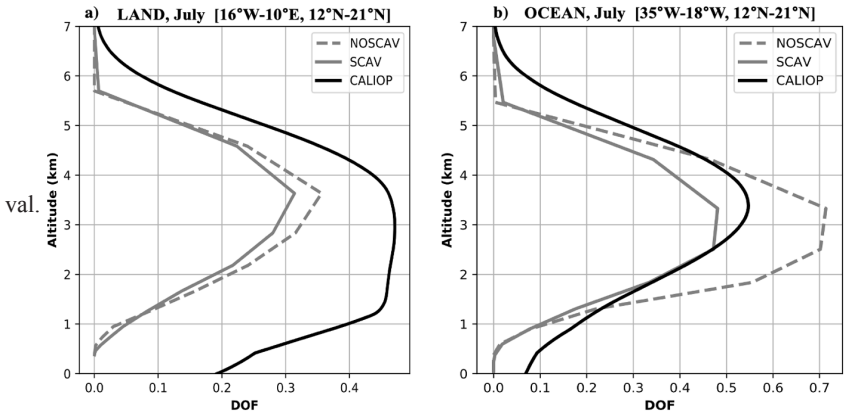

val.

Figure 5. Comparison of July vertical distribution of dust vertical frequency obtained from CALIOP observations (black lines), SCAV (gray lines), and NOSCAV (gray dashed lines) experiments for 2006–2010: (a) over the land (16°W–10°E) and (b) over the ocean (35°W–18°W).

In July, CODU is transported upward up to 600 hPa (4 km) overland by boundary layer turbulence and dry convection, represented in the model by the turbulent diffusion and the thermal plumes (not shown). The turbulent diffusion of the boundary layer raises the dust emitted at the surface up to 950 hPa, while the vertical transport to 800 hPa (2 km) is made by the thermal plumes (not shown). In the simulations, the effect of the monsoon flux on the dust vertical distribution is clearly shown by the negative advection tendency between the surface and 900 hPa (below 1 km), which is consistent with previous studies [68,80,86]. In higher levels of the atmosphere, the deep convective tendencies dominate the vertical transport. It will be detailed in the next section.

Larger size particles are redistributed in the atmosphere from the SAL (around 700 hPa) before being deposited at the surface by the sedimentation process. The latter is more important than the dynamical process below 900 hPa with a tendency respectively of –2 for sedimentation and –0.9 $g.kg^{-1}.day^{-1}$ for dynamical processes (**Figure 6b**). Above the ocean (**Figure 6d**), the large-scale scavenging effect redistributes dust between the surface and 950 hPa. The latter shows an important effect of the advection tendency in the SAL between 500 and 900 hPa (1 and 5 km) in agreement with the dust occurrence over the ocean in summer (**Figure 3d**) and the CALIOP observations (**Figure 3c**). Large particles are also transported far from the dust sources in the high altitudes between (500 and 800 hPa) in agreement with the observations from the Fennec campaign [27].

3.5 Control by deep convection

Our analysis is focused in this section on the mechanisms controlling the vertical distribution of CODU and FINE dust inside the ITCZ during summer over West Africa (**Figure 7**). Inside the grid-box selected in **Figure 7**, the dust is transported by advection in the upper part of the SAL (500 and 750 hPa) (**Figures 7a and 7b**) corresponding to the altitude between 2.5 and 5 km where the maximum DOF has been found with CALIOP (**Figure 3c**). This strong dust advection is shown by a positive value of the tendency with a maximum of 0.04 $g.kg^{-1}.day^{-1}$ in the south part of the African Easterly Jet (AEJ) (600 and 700 hPa above 3 km) (**Figure 7b**). At this altitude, the removal of dust by the combination of sedimentation, stratiform precipitation (600 and 950 hPa), and convective rainfall is less important than the advection. Between 750 and 900 hPa (1 and 3 km), the dust originates from the sedimentation effect (**Figure 7b**), convective transport and the re-evaporation of the unsaturated drafts (**Figure 7d**) is removed by the large-scale scavenging (**Figures 7b and 7d**). In western Africa, the model has a strong large-scale tendency to concentrate dust at lower levels between 950 hPa and surface (**Figure 7d**). However, the impact of the atmospheric boundary layer is very strong and brings dust up to 4 km (600 hPa) (**Figure 7b**). **Figure 7c** shows the same behavior in terms of convection and large-scale circulation but FINE is not affected by the sedimentation. **Figures 7c and 7d** show that the convective transport moves a part of dust from the SAL between 500–750 hPa (3 and 5 km) to high altitudes between 100 and 350 hPa (8 and 16 km) with a maximum contribution around of 200 hPa (12 km). However, the import of dust by convection is almost canceled: Dust is removed by the saturated updrafts combined with the effect of large-scale scavenging (**Figures 7c and 7d**). Strong activity of the convection removes a large part of dust contained in the side part of the AEJ between 500 and 900 hPa (1 and 5 km) but the unsaturated downdraft redistributes dust between 3 and 4 km (**Figure 7d**).

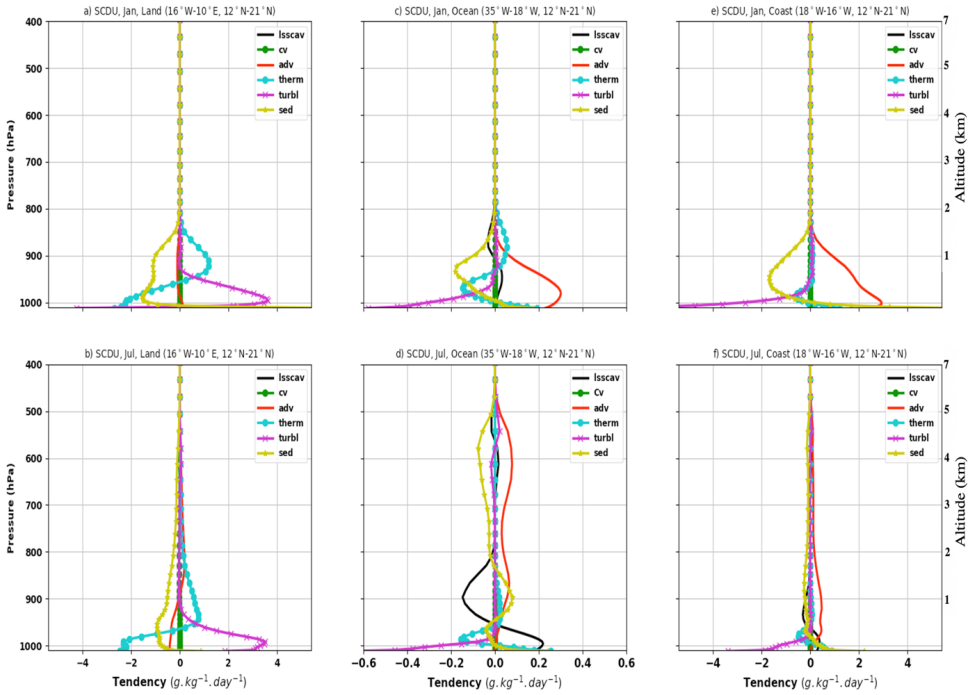

Figure 6. January (top) and July (bottom) vertical profiles of the different terms (g.kg^{-1}.day^{-1}) controlling the dust evolution in the SCAV LMDZ experiment averaged between 2006 and 2010 overland (a and b; 16°W–10°W), ocean (c and d; 35°W–20°W) and around the coast (e and f; 18°W–16°W). The large-scale scavenging (lsscav) corresponds to black solid lines, the convective scavenging combined with the vertical transport (cv) is shown by the green lines with dot markers, the advection (adv) is represented by the red lines, the thermal plume (therm) is shown by cyan solid lines with dot markers, the boundary layer turbulence diffusion (turbl) by magenta solid with markers, and the sedimentation (sed) in yellow with star markers.

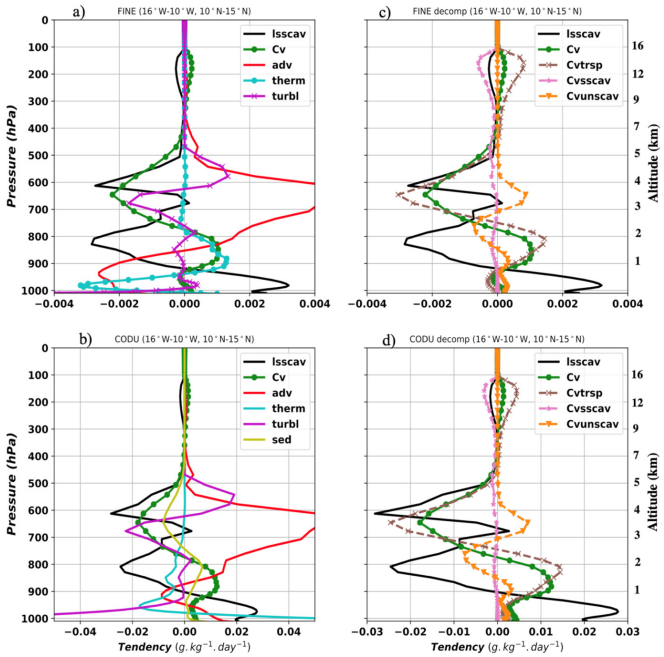

Figure 7. Simulated vertical tendencies of CODU (a) and FINE (b) in July 2006–2010. The plots are made in the convectively active domain (10°N-15°N) for zonal cross-sections (16°W–10°W). In panels (a), (b), the lsscav tendency is in black solid lines, the advection (adv) red solid lines, the Cv (green lines with dot markers), the term in cyan with dot markers, the turbl (magenta with star markers), and sed (yellow solid lines). Panels (c), (d) show the lsscav (black solid lines) and the total Cv of the simulation which is separated into three tendencies: Vertical transport (Cvtrsp) in dashed brown line with markers, the saturated updraft (Cvsscav) in dashed magenta lines with star markers, and unsaturated downdraft (Cvunscav) in orange with star markers.

4. Discussion

The comparison of two configurations of the LMDZ model with satellites and ground observations reveals a bias in the simulated AOD showing the importance of representing deep convective scavenging in models used for research on dust. This uncertainty is related to the accumulation of dust in the atmosphere during the boreal summer (**Figures 3c, 3d and 3e**). The combination of intense activity of the Saharan dust sources and the absence of precipitation in the model increases the AOD of dust. The overestimation of AOD with the SCAV simulation in Dakar is due to the strong dust emission of the model on the West African coast in agreement with Hourdin et al. (2015). The comparison of LMDZ's AOD in Escribano et al. (2016) [24] shows that the coastal dust sources are well represented in the model during the whole year. Our results are in accordance with previous studies [65,87]. Messager et al. (2010) have shown that intense surface heating from solar radiation (so-called heat low) controls dry convection processes which contribute about 35% of the global dust budget [24,88]. This study has also identified the processes involved in the control of the vertical distribution of mineral dust in West Africa. The advection in the SAL is reproduced by the model as shown by the vertical profile of dust over the ocean which slightly underestimates the vertical profile between the surface and around 1.5 km. The collocation of the maximum DOF in the SAL (**Figure 3d**) with a maximum wind speed (**Figures 7a and 7b**) by the model simulations near the West African coast is in agreement with the findings of Tsamalis et al. (2013) [68]. **Figures 6b–6d** and **Figures 7a and 7b** show a location of the AEJ above 3 km during summer in agreement with observed data [68]. The weak dry deposition of CODU and FINE between land and ocean could be related to their intrusion in the SAL. The removal effect of large-scale scavenging between 1 and 3 km (**Figures 7b and 7d**) and the good agreement of the model's AOD in the summer season (**Figure 1**) show that the underestimation of the DOF below 3 km (**Figure 5a**) for SCAV could be attributed to the negative effect of stratiform precipitation. The changes noticed in the dust occurrence for the model between land and ocean are essentially explained by the strong activity of the dynamical processes (advection) inside the SAL between 2 and 5 km for SCDU (**Figure 6d**) associated with the weak effect of the sedimentation for CODU (**Figure 7b**) and low precipitations (**Figure 6d**). This result is in agreement with the findings of Vuolo et al. (2009) [69]. Finally, it should be noted that our simulations are relatively short given the documented interannual and decadal variability in dust emissions and transport. However, we intend to perform a larger set of ensemble simulations over a longer period to overcome the limitations of a two short simulation study and to be able to improve vertical dust transport diagnostic and statistics.

5. Conclusions

The online implementation of the SPLA module coupled with the LMDZ GCM makes it possible to organize the dust size in three bins and to discriminate the different contributions of the physical processes as tendencies. This paper focuses on the vertical distribution of mineral dust and on the mechanisms impacting their redistribution in the troposphere in particular over Western-North Africa inside the (5°N–15°N; 16°W–10°W) domain, during the monsoon season, where deep convection was dominant. The results show that the LMDZ model has the skill to reproduce a clear seasonal cycle of AOD when all the physical processes listed are activated in the model. By deactivating scavenging, we show the importance of this specific process, as well as the importance of processed-based transport and scavenging in a deep convective parameterization on the dust seasonal cycle and vertical distribution of Saharan dust. Deep convection contributes to increasing atmospheric dust loading around 650 hPa (3.5 km) and 900 hPa (1 km). While scavenging processes are always considered as a sink for aerosols, it is shown here that convection can locally increase the dust concentration by the re-evaporation of the unsaturated downdraft. The effects of large-scale scavenging due to the re-evaporation of the strati-

form precipitation are seen mostly activated between the surface and 900 hPa. Above the dry convection region around 20°N, the intertropical discontinuity signal is clearly shown near the surface and explained by the convergence between Harmattan and monsoon flux. Moreover, the vertical distribution of dust is limited above the top dust layer by the large-scale subsidence of air masses due to the Hadley cell. Vertical transport of dust is clearly shown in North Africa around the latitude 10°N. The elevation of the dust layer on the eastern side of the Atlantic Ocean is mostly due to the marine boundary layer rather than the dynamic effects. Differences in the vertical profiles of dust occurrence frequency between the model and CALIPSO aerosol types show that the LMDZ model reproduces reasonably well the vertical transport and the advection but underestimates the dust mass concentration over North Africa below 3 km due to stratiform precipitation. The elevation of the SAL above the Atlantic Ocean starts at the transitional zone between land and ocean in the satellite observations and model simulations. This study brings to light that the elevation of dust near the western African coast, which previously has been only attributed to the dynamics of the monsoon flux, may be more affected by marine boundary layer processes. The large dust occurrence in the West Africa area during the summer season, due to the higher activity of the dust sources, is reproduced by model simulations. The study also points out a connection between the intertropical discontinuity (ITD) and the ITCZ overland in summer, inducing a vertical transport of mineral dust in the Sahara.

Conflict of Interest

There is no conflict of interest.

Acknowledgments

The authors wish to thank the Ecosystem Approach to the management of fisheries and the marine environment in the West African Waters (AWA) project. They also acknowledge support from the international joint laboratory ECLAIRS. The Laboratoire de Météorologie Dynamique (LMD) and the Global Challenges Research Fund (GCRF) African Science for Weather Information and Techniques (SWIFT) Programme. NASA, CNES, and ICARE are acknowledged for providing access to CALIOP and Sun photometer AERONET data.

References

[1] Washington, R., Todd, M.C., Engelstaedter, S., et al., 2006. Dust and the low-level circulation over the Bodélé Depression, Chad: Observations from BoDEx 2005. Journal of Geophysical Research: Atmospheres. 111(D3).
DOI: https://doi.org/10.1029/2005JD006502

[2] Haustein, K., Pérez, C., Baldasano, J.M., et al., 2009. Regional dust model performance during SAMUM 2006. Geophysical Research Letters. 36(3).
DOI: https://doi.org/10.1029/2008GL036463

[3] Kaufman, Y.J., Koren, I., Remer, L.A., et al., 2005. Dust transport and deposition observed from the Terra-Moderate Resolution Imaging Spectroradiometer (MODIS) spacecraft over the Atlantic Ocean. Journal of Geophysical Research: Atmospheres. 110(D10).
DOI: https://doi.org/10.1029/2003JD004436

[4] Senghor, H., Roberts, A.J., Dieng, A.L., et al., 2021. Transport and deposition of Saharan dust observed from satellite images and ground measurements. Journal of Atmospheric Science Research. 4(2), 1–11.
DOI: https://doi.org/10.30564/jasr.v4i2.3165

[5] Diokhane, A.M., Jenkins, G.S., Manga, N., et al., 2016. Linkages between observed, modeled Saharan dust loading and meningitis in Senegal during 2012 and 2013. International Journal of Biometeorology. 60, 557–575.
DOI: https://doi.org/10.1007/s00484-015-1051-5

[6] Samoli, E., Stafoggia, M., Rodopoulou, S., et al., 2013. Associations between fine and coarse particles and mortality in Mediterranean cities: Results from the MED-PARTICLES project. Environmental Health Perspectives. 121(8), 932–938.

DOI: http://dx.doi.org/10.1289/ehp.1206124

[7] Yu, H., Tan, Q., Zhou, L., et al., 2021. Observation and modeling of the historic "Godzilla" African dust intrusion into the Caribbean Basin and the southern US in June 2020. Atmospheric Chemistry and Physics. 21(16), 12359–12383. DOI: https://doi.org/10.5194/acp-21-12359-2021

[8] Creamean, J.M., Suski, K.J., Rosenfeld, D., et al., 2013. Dust and biological aerosols from the Sahara and Asia influence precipitation in the western US. Science. 339(6127), 1572–1578.

[9] Sokolik, I.N., Toon, O.B., 1999. Incorporation of mineralogical composition into models of the radiative properties of mineral aerosol from UV to IR wavelengths. Journal of Geophysical Research: Atmospheres. 104(D8), 9423–9444. DOI: https://doi.org/10.1029/1998JD200048

[10] Balkanski, Y., Bonnet, R., Boucher, O., et al., 2021. Dust induced atmospheric absorption improves tropical precipitations in climate models. Atmospheric Chemistry and Physics Discussions. DOI: https://doi.org/10.5194/acp-2021-12

[11] Engelstaedter, S., Tegen, I., Washington, R., 2006. North African dust emissions and transport. Earth-Science Reviews. 79(1–2), 73–100. DOI: https://doi.org/10.1016/j.earscirev.2006.06.004

[12] Hourdin, F., Gueye, M., Diallo, B., et al., 2015. Parameterization of convective transport in the boundary layer and its impact on the representation of the diurnal cycle of wind and dust emissions. Atmospheric Chemistry and Physics. 15(12), 6775–6788. DOI: https://doi.org/10.5194/acp-15-6775-2015

[13] Allen, C.J., Washington, R., Engelstaedter, S., 2013. Dust emission and transport mechanisms in the central Sahara: Fennec ground-based observations from Bordj Badji Mokhtar, June 2011. Journal of Geophysical Research: Atmospheres. 118(12), 6212–6232. DOI: https://doi.org/10.1002/jgrd.50534

[14] Miller, S.D., Kuciauskas, A.P., Liu, M., et al., 2008. Haboob dust storms of the southern Arabian Peninsula. Journal of Geophysical Research: Atmospheres. 113(D1). DOI: https://doi.org/10.1029/2007JD008550

[15] Tost, H., Jöckel, P., Lelieveld, J., 2006. Influence of different convection parameterisations in a GCM. Atmospheric Chemistry and Physics. 6(12), 5475–5493. DOI: https://doi.org/10.5194/acp-6-5475-2006

[16] Tost, H., Lawrence, M.G., Brühl, C., et al., 2010. Uncertainties in atmospheric chemistry modelling due to convection parameterisations and subsequent scavenging. Atmospheric Chemistry and Physics. 10(4), 1931–1951. DOI: https://doi.org/10.5194/acp-10-1931-2010

[17] Pilon, R., Grandpeix, J.Y., Heinrich, P., 2015. Representation of transport and scavenging of trace particlesin the Emanuel moist convection scheme. Quarterly Journal of the Royal Meteorological Society. 141(689), 1244–1258. DOI: https://doi.org/10.1002/qj.2431

[18] Knippertz, P., Stuut, J.B.W., 2014. Introduction. Mineral dust. Springer: Dordrecht. pp. 1–14. DOI: https://doi.org/10.1007/978-94-017-8978-3_1

[19] Malavelle, F., Pont, V., Mallet, M., et al., 2011. Simulation of aerosol radiative effects over West Africa during DABEX and AMMA SOP-0. Journal of Geophysical Research: Atmospheres. 116(D8). DOI: https://doi.org/10.1029/2010JD014829

[20] Solmon, F., Elguindi, N., Mallet, M., 2012. Radiative and climatic effects of dust over West Africa, as simulated by a regional climate model. Climate Research. 52, 97–113. DOI: https://doi.org/10.3354/cr01039

[21] Ji, Z., Wang, G., Pal, J.S., et al., 2016. Potential climate effect of mineral aerosols over West Africa. Part I: model validation and contemporary climate evaluation. Climate Dynamics. 46, 1223–1239. DOI: https://doi.org/10.1007/s00382-015-2641-y

[22] Schmechtig, C., Marticorena, B., Chatenet, B., et al., 2011. Simulation of the mineral dust content over Western Africa from the event to

the annual scale with the CHIMERE-DUST model. Atmospheric Chemistry and Physics. 11(14), 7185–7207.
DOI: https://doi.org/10.5194/acp-11-7185-2011

[23] Pérez, C., Haustein, K., Janjic, Z., et al., 2011. Atmospheric dust modeling from meso to global scales with the online NMMB/BSC-Dust model—Part 1: Model description, annual simulations and evaluation. Atmospheric Chemistry and Physics. 11(24), 13001–13027.
DOI: https://doi.org/10.5194/acp-11-13001-2011

[24] Escribano, J., Boucher, O., Chevallier, F., et al., 2016. Subregional inversion of North African dust sources. Journal of Geophysical Research: Atmospheres. 121(14), 8549–8566.
DOI: https://doi.org/10.1002/2016JD025020

[25] Hu, Z., Huang, J., Zhao, C., et al., 2020. Modeling dust sources, transport, and radiative effects at different altitudes over the Tibetan Plateau. Atmospheric Chemistry and Physics. 20(3), 1507–1529.
DOI: https://doi.org/10.5194/acp-20-1507-2020

[26] Kallos, G., Papadopoulos, A., Katsafados, P., et al., 2006. Transatlantic Saharan dust transport: Model simulation and results. Journal of Geophysical Research: Atmospheres. 111(D9).
DOI: https://doi.org/10.1029/2005JD006207

[27] Ryder, C.L., Highwood, E.J., Lai, T.M., et al., 2013. Impact of atmospheric transport on the evolution of microphysical and optical properties of Saharan dust. Geophysical Research Letters. 40(10), 2433–2438.
DOI: https://doi.org/10.1002/grl.50482

[28] Gasteiger, J., Wiegner, M., Groß, S., et al., 2011. Modelling lidar-relevant optical properties of complex mineral dust aerosols. Tellus B. 63(4), 725–741.
DOI: https://doi.org/10.1111/j.1600-0889.2011.00559.x

[29] Adebiyi, A.A., Kok, J.F., Wang, Y., et al., 2020. Dust Constraints from joint Observational-Modelling-experiMental analysis (DustCOMM): Comparison with measurements and model simulations. Atmospheric Chemistry and Physics. 20(2), 829–863.
DOI: https://doi.org/10.5194/acp-20-829-2020

[30] Liu, H., Jacob, D.J., Bey, I., et al., 2001. Constraints from ^{210}Pb and ^{7}Be on wet deposition and transport in a global three-dimensional chemical tracer model driven by assimilated meteorological fields. Journal of Geophysical Research: Atmospheres. 106(D11), 12109–12128.
DOI: https://doi.org/10.1029/2000JD900839

[31] Heinrich, P., Jamelot, A., 2011. Atmospheric transport simulation of ^{210}Pb and ^{7}Be by the LMDz general circulation model and sensitivity to convection and scavenging parameterization. Atmospheric Research. 101(1–2), 54–66.
DOI: https://doi.org/10.1016/j.atmosres.2011.01.008

[32] Heinrich, P., Pilon, R., 2013. Simulation of ^{210}Pb and ^{7}Be scavenging in the tropics by the LMDz general circulation model. Atmospheric Research. 132, 490–505.
DOI: https://doi.org/10.1016/j.atmosres.2013.07.004

[33] Hourdin, F., Rio, C., Grandpeix, J.Y., et al., 2020. LMDZ6A: The atmospheric component of the IPSL climate model with improved and better tuned physics. Journal of Advances in Modeling Earth Systems. 12(7), e2019MS001892.
DOI: https://doi.org/10.1029/2019MS001892

[34] Grandpeix, J.Y., Phillips, V., Tailleux, R., 2004. Improved mixing representation in Emanuel's convection scheme. Quarterly Journal of the Royal Meteorological Society. 130(604), 3207–3222.
DOI: https://doi.org/10.1256/qj.03.144

[35] Emanuel, K.A., 1991. A scheme for representing cumulus convection in large-scale models. Journal of the Atmospheric Sciences. 48(21), 2313–2329.
DOI: https://doi.org/10.1175/1520-0469(1991)048<2313:ASFRCC>2.0.CO;2

[36] Grandpeix, J.Y., Lafore, J.P., 2010. A density current parameterization coupled with Eman-

uel's convection scheme. Part I: The models. Journal of the Atmospheric Sciences. 67(4), 881–897.
DOI: https://doi.org/10.1175/2009JAS3044.1

[37] Grandpeix, J.Y., Lafore, J.P., Cheruy, F., 2010. A density current parameterization coupled with Emanuel's convection scheme. Part II: 1D simulations. Journal of the Atmospheric Sciences. 67(4), 898–922.
DOI: https://doi.org/10.1175/2009JAS3045.1

[38] Rochetin, N., Couvreux, F., Grandpeix, J.Y., et al., 2014. Deep convection triggering by boundary layer thermals. Part I: LES analysis and stochastic triggering formulation. Journal of the Atmospheric Sciences. 71(2), 496–514.
DOI: https://doi.org/10.1175/JAS-D-12-0336.1

[39] Hourdin, F., Jam, A., Rio, C., et al., 2019. Unified parameterization of convective boundary layer transport and clouds with the thermal plume model. Journal of Advances in Modeling Earth Systems. 11(9), 2910–2933.
DOI: https://doi.org/10.1029/2019MS001666

[40] Le Trent, H., Li, Z.X., 1991. Sensitivity of an atmospheric general circulation model to prescribed SST changes: Feedback effects associated with the simulation of cloud optical properties. Climate Dynamics. 5, 175–187.

[41] Coindreau, O., Hourdin, F., Haeffelin, M., et al., 2007. Assessment of physical parameterizations using a global climate model with stretchable grid and nudging. Monthly Weather Review. 135(4), 1474–1489.
DOI: https://doi.org/10.1175/MWR3338.1

[42] Hourdin, F., Grandpeix, J.Y., Rio, C., et al., 2013. LMDZ5B: The atmospheric component of the IPSL climate model with revisited parameterizations for clouds and convection. Climate Dynamics. 40, 2193–2222.
DOI: https://doi.org/10.1007/s00382-012-1343-y

[43] Wang, F., Ducharne, A., Cheruy, F., et al., 2018. Impact of a shallow groundwater table on the global water cycle in the IPSL land–atmosphere coupled model. Climate Dynamics. 50, 3505–3522.
DOI: https://doi.org/10.1007/s00382-017-3820-9

[44] Krinner, G., Viovy, N., de Noblet-Ducoudré, N., et al., 2005. A dynamic global vegetation model for studies of the coupled atmosphere-biosphere system. Global Biogeochemical Cycles. 19(1).
DOI: https://doi.org/10.1029/2003GB002199

[45] Cheruy, F., Ducharne, A., Hourdin, F., et al., 2020. Improved near-surface continental climate in IPSL-CM6A-LR by combined evolutions of atmospheric and land surface physics. Journal of Advances in Modeling Earth Systems. 12(10), e2019MS002005.
DOI: https://doi.org/10.1029/2019MS002005

[46] Marticorena, B., Chatenet, B., Rajot, J.L., et al., 2010. Temporal variability of mineral dust concentrations over West Africa: Analyses of a pluriannual monitoring from the AMMA Sahelian Dust Transect. Atmospheric Chemistry and Physics. 10(18), 8899–8915.
DOI: https://doi.org/10.5194/acp-10-8899-2010

[47] Dee, D.P., Uppala, S.M., Simmons, A.J., et al., 2011. The ERA-Interim reanalysis: Configuration and performance of the data assimilation system. Quarterly Journal of the Royal Meteorological Society. 137(656), 553–597.
DOI: https://doi.org/10.1002/qj.828

[48] Hersbach, H., Bell, B., Berrisford, P., et al., 2020. The ERA5 global reanalysis. Quarterly Journal of the Royal Meteorological Society. 146(730), 1999–2049.
DOI: https://doi.org/10.1002/qj.3803

[49] Huneeus, N., Chevallier, F., Boucher, O., 2012. Estimating aerosol emissions by assimilating observed aerosol optical depth in a global aerosol model. Atmospheric Chemistry and Physics. 12(10), 4585–4606.
DOI: https://doi.org/10.5194/acp-12-4585-2012

[50] Menut, L., Pérez, C., Haustein, K., et al., 2013. Impact of surface roughness and soil texture on mineral dust emission fluxes modeling. Journal of Geophysical Research: Atmospheres. 118(12), 6505–6520.

DOI: https://doi.org/10.1002/jgrd.50313

[51] Marticorena, B., Bergametti, G., 1995. Modeling the atmospheric dust cycle: 1. Design of a soil-derived dust emission scheme. Journal of Geophysical Research: Atmospheres. 100(D8), 16415–16430.
DOI: https://doi.org/10.1029/95JD00690

[52] Alfaro, S.C., Gomes, L., 2001. Modeling mineral aerosol production by wind erosion: Emission intensities and aerosol size distributions in source areas. Journal of Geophysical Research: Atmospheres. 106(D16), 18075–18084.
DOI: https://doi.org/10.1029/2000JD900339

[53] Shao, Y., Lu, H., 2000. A simple expression for wind erosion threshold friction velocity. Journal of Geophysical Research: Atmospheres. 105(D17), 22437–22443.
DOI: https://doi.org/10.1029/2000JD900304

[54] Marticorena, B., Bergametti, G., Aumont, B., et al., 1997. Modeling the atmospheric dust cycle: 2. Simulation of Saharan dust sources. Journal of Geophysical Research: Atmospheres. 102(D4), 4387–4404.
DOI: https://doi.org/10.1029/96JD02964

[55] Huneeus, N., Boucher, O., Chevallier, F., 2009. Simplified aerosol modeling for variational data assimilation. Geoscientific Model Development. 2(2), 213–229.
DOI: https://doi.org/10.5194/gmd-2-213-2009

[56] Reddy, M.S., Boucher, O., 2004. A study of the global cycle of carbonaceous aerosols in the LMDZT general circulation model. Journal of Geophysical Research: Atmospheres. 109(D14).
DOI: https://doi.org/10.1029/2003JD004048

[57] Hourdin, F., Armengaud, A., 1999. The use of finite-volume methods for atmospheric advection of trace species. Part I: Test of various formulations in a general circulation model. Monthly Weather Review. 127(5), 822–837.
DOI: https://doi.org/10.1175/1520-0493(1999)127<0822:TUOFVM>2.0.CO;2

[58] Yamada, T., 1983. Simulations of nocturnal drainage flows by a q2l turbulence closure model. Journal of the Atmospheric Sciences. 40(1), 91–106.
DOI: https://doi.org/10.1175/1520-0469(1983)040<0091:SONDFB>2.0.CO;2

[59] Holben, B.N., Eck, T.F., Slutsker, I.A., et al., 1998. AERONET—A federated instrument network and data archive for aerosol characterization. Remote Sensing of Environment. 66(1), 1–16.
DOI: https://doi.org/10.1016/S0034-4257(98)00031-5

[60] Léon, J.F., Derimian, Y., Chiapello, I., et al., 2009. Aerosol vertical distribution and optical properties over M'Bour (16.96° W; 14.39° N), Senegal from 2006 to 2008. Atmospheric Chemistry and Physics. 9(23), 9249–9261.
DOI: https://doi.org/10.5194/acp-9-9249-2009

[61] Hunt, W.H., Winker, D.M., Vaughan, M.A., et al., 2009. CALIPSO lidar description and performance assessment. Journal of Atmospheric and Oceanic Technology. 26(7), 1214–1228.
DOI: https://doi.org/10.1175/2009JTECHA1223.1

[62] Winker, D.M., Hunt, W.H., McGill, M.J., 2007. Initial performance assessment of CALIOP. Geophysical Research Letters. 34(19).
DOI: https://doi.org/10.1029/2007GL030135

[63] Winker, D.M., Pelon, J.R., McCormick, M.P., 2003. CALIPSO mission: Spaceborne lidar for observation of aerosols and clouds. Lidar Remote Sensing for Industry and Environment Monitoring III. 4893, 1–11.
DOI: https://doi.org/10.1117/12.466539

[64] Liu, Z., Vaughan, M., Winker, D., et al., 2009. The CALIPSO lidar cloud and aerosol discrimination: Version 2 algorithm and initial assessment of performance. Journal of Atmospheric and Oceanic Technology. 26(7), 1198–1213.
DOI: https://doi.org/10.1175/2009JTECHA1229.1

[65] Senghor, H., Machu, É., Hourdin, F., et al., 2017. Seasonal cycle of desert aerosols in western Africa: Analysis of the coastal transition with passive and active sensors. Atmospheric Chemistry and Physics. 17(13), 8395–8410.

DOI: https://doi.org/10.5194/acp-17-8395-2017

[66] Adams, A.M., Prospero, J.M., Zhang, C., 2012. CALIPSO-derived three-dimensional structure of aerosol over the Atlantic Basin and adjacent continents. Journal of Climate. 25(19), 6862–6879.
DOI: https://doi.org/10.1175/JCLI-D-11-00672.1

[67] Schuster, G.L., Vaughan, M., MacDonnell, D., et al., 2012. Comparison of CALIPSO aerosol optical depth retrievals to AERONET measurements, and a climatology for the lidar ratio of dust. Atmospheric Chemistry and Physics. 12(16), 7431–7452.
DOI: https://doi.org/10.5194/acp-12-7431-2012

[68] Tsamalis, C., Chédin, A., Pelon, J., et al., 2013. The seasonal vertical distribution of the Saharan Air Layer and its modulation by the wind. Atmospheric Chemistry and Physics. 13(22), 11235–11257.
DOI: https://doi.org/10.5194/acp-13-11235-2013

[69] Vuolo, M.R., Chepfer, H., Menut, L., et al., 2009. Comparison of mineral dust layers vertical structures modeled with CHIMERE-DUST and observed with the CALIOP lidar. Journal of Geophysical Research: Atmospheres. 114(D9).
DOI: https://doi.org/10.1029/2008JD011219

[70] Wallace, J.M., Hobbs, P.V., 2006. Atmospheric science: An introductory survey (Vol. 92). Elsevier: Amsterdam.

[71] Weinzierl, B., Ansmann, A., Prospero, J.M., et al., 2017. The Saharan aerosol long-range transport and aerosol–cloud-interaction experiment: overview and selected highlights. Bulletin of the American Meteorological Society. 98(7), 1427–1451.
DOI: https://doi.org/10.1175/BAMS-D-15-00142.1

[72] Prospero, J.M., Ginoux, P., Torres, O., et al., 2002. Environmental characterization of global sources of atmospheric soil dust identified with the Nimbus 7 Total Ozone Mapping Spectrometer (TOMS) absorbing aerosol product. Reviews of Geophysics. 40(1), 21–31.
DOI: https://doi.org/10.1029/2000RG000095

[73] Cuesta, J., Marsham, J.H., Parker, D.J., et al., 2009. Dynamical mechanisms controlling the vertical redistribution of dust and the thermodynamic structure of the West Saharan atmospheric boundary layer during summer. Atmospheric Science Letters. 10(1), 34–42.
DOI: https://doi.org/10.1002/asl.207

[74] Ansmann, A., Petzold, A., Kandler, K., et al., 2011. Saharan mineral dust experiments SAMUM–1 and SAMUM–2: What have we learned? Tellus B. 63(4), 403–429.
DOI: https://doi.org/10.1111/j.1600-0889.2011.00555.x

[75] Hamilton, R.A., Archbold, J.W., Douglas, C.K.M., 1945. Meteorology of Nigeria and adjacent territory. Quarterly Journal of the Royal Meteorological Society. 71(309–310), 231–264.
DOI: https://doi.org/10.1002/qj.49707130905

[76] Stuut, J.B., Zabel, M., Ratmeyer, V., et al., 2005. Provenance of present-day eolian dust collected off NW Africa. Journal of Geophysical Research: Atmospheres. 110(D4).
DOI: https://doi.org/10.1029/2004JD005161

[77] Ozer, P., Laghdaf, M.B.O.M., Lemine, S.O.M., et al., 2007. Estimation of air quality degradation due to Saharan dust at Nouakchott, Mauritania, from horizontal visibility data. Water, Air, and Soil Pollution. 178, 79–87.
DOI: https://doi.org/10.1007/s11270-006-9152-8

[78] Yu, H., Chin, M., Yuan, T., et al., 2015. The fertilizing role of African dust in the Amazon rainforest: A first multiyear assessment based on data from Cloud-Aerosol Lidar and Infrared Pathfinder Satellite Observations. Geophysical Research Letters. 42(6), 1984–1991.
DOI: https://doi.org/10.1002/2015GL063040

[79] Goudie, A.S., Middleton, N.J., 2001. Saharan dust storms: Nature and consequences. Earth-Science Reviews. 56(1–4), 179–204.
DOI: https://doi.org/10.1016/S0012-8252(01)00067-8

[80] Bou Karam, D., Flamant, C., Knippertz, P., et al.,

2008. Dust emissions over the Sahel associated with the West African monsoon intertropical discontinuity region: A representative case-study. Quarterly Journal of the Royal Meteorological Society. 134(632), 621–634.
DOI: https://doi.org/10.1002/qj.244

[81] Knippertz, P., Todd, M.C., 2010. The central west Saharan dust hot spot and its relation to African easterly waves and extratropical disturbances. Journal of Geophysical Research: Atmospheres. 115(D12).
DOI: https://doi.org/10.1029/2009JD012819

[82] Tegen, I., Schepanski, K., Heinold, B., 2013. Comparing two years of Saharan dust source activation obtained by regional modelling and satellite observations. Atmospheric Chemistry and Physics. 13(5), 2381–2390.
DOI: https://doi.org/10.5194/acp-13-2381-2013

[83] Chiapello, I., Bergametti, G., Gomes, L., et al., 1995. An additional low layer transport of Sahelian and Saharan dust over the north-eastern tropical Atlantic. Geophysical Research Letters. 22(23), 3191–3194.
DOI: https://doi.org/10.1029/95GL03313

[84] Liu, D., Wang, Y., Wang, Z., et al., 2012. The three-dimensional structure of transatlantic African dust transport: A new perspective from CALIPSO LIDAR measurements. Advances in Meteorology. 850704.
DOI: https://doi.org/10.1155/2012/850704

[85] Friese, C.A., van der Does, M., Merkel, U., et al., 2016. Environmental factors controlling the seasonal variability in particle size distribution of modern Saharan dust deposited off Cape Blanc. Aeolian Research. 22, 165–179.
DOI: https://doi.org/10.1016/j.aeolia.2016.04.005

[86] Schepanski, K., Tegen, I., Laurent, B., et al., 2007. A new Saharan dust source activation frequency map derived from MSG-SEVIRI IR-channels. Geophysical Research Letters. 34(18).
DOI: https://doi.org/10.1029/2007GL030168

[87] Lavaysse, C., Flamant, C., Janicot, S., et al., 2009. Seasonal evolution of the West African heat low: A climatological perspective. Climate Dynamics. 33, 313–330.
DOI: https://doi.org/10.1007/s00382-009-0553-4

[88] Messager, C., Parker, D.J., Reitebuch, O., et al., 2010. Structure and dynamics of the Saharan atmospheric boundary layer during the West African monsoon onset: Observations and analyses from the research flights of 14 and 17 July 2006. Quarterly Journal of the Royal Meteorological Society. 136(S1), 107–124.
DOI: https://doi.org/10.1002/qj.469